Fuel Processing Technology 281 (2026) 108364

Contents lists available at ScienceDirect

Fuel Processing Technology

journal homepage: www.elsevier.com/locate/fuproc

Research article

Selective hydrocracking of polystyrene waste over Pt- and Ru-supported zeolite catalysts into high yield LPG and ethylbenzene

Olajumoke Alabi-Babalola [a,b,*], Edidiong Asuquo [a], Hassan Alhassawi [a], Mujtba Alnasser [a], Amal Nadri [a], Sarayute Chansai [a], Carmine D'Agostino [a,c,*], Arthur Garforth [a,*]

[a] Department of Chemical Engineering, School of Engineering, University of Manchester, Oxford Road, Manchester, M13 9PL, UK
[b] Department of Chemical Engineering, Obafemi Awolowo University, Ile-Ife, Nigeria
[c] Dipartimento di Ingegneria Civile, Chimica, Ambientale e dei Materiali (DICAM), Alma Mater Studiorum – Universita` di Bologna, Via Terracini, 28, 40131 Bologna, Italy

ARTICLE INFO

Keywords:
Polystyrene waste
Catalytic cracking
Hydrocracking
Zeolite catalysts
Circular economy
Gas chromatography

ABSTRACT

This work investigates the chemical upcycling of non-biodegradable polystyrene waste into useful industrial products via catalytic hydrocracking. Zeolite-Y and ZSM-5 catalysts were impregnated with platinum and ruthenium and used in the conversion of polystyrene waste into the highly-desirable liquified natural gases and liquid ethylbenzene. Reactions carried out in a Parr reactor gave $C_3 - C_4$ gas selectivity of 60–67% for Pt-doped and 41–74 % for Ru-doped HY catalyst, while the Pt-doped ZSM-5 gave 94–96% $C_2 - C_4$ selectivity of the total gas products. Liquid analysis revealed both Pt and Ru were selective towards single-ring aromatics, notably ethylbenzene: 37–44%. However, Pt-ZSM-5 gave negligible liquid products due to its relatively larger pore sizes (3.8 nm) which promotes faster mass transport leading to more cracking and less secondary reactions. Higher pressures significantly increased feedstock to fluid conversion from 37 to 73% at 15 and 25 bar H_2 respectively. Longer reaction times and lower polymer : catalyst ratios enhanced hydrogenation and ring opening reactions to give lower molecular weight compounds $\leq C_8$ and cycloalkanes. Spent catalysts were reused four times and similar ethylbenzene selectivity obtained, hence indicating excellent catalyst stability. We present a waste management control strategy in the feedstock recycling of plastic waste using bifunctional catalysts to produce fuels, whilst promoting alternative sources to the growing energy demand and environmentally benign synthetic routes in the petrochemical industry.

1. Introduction

Rapid global industrialization has led to the production of low-cost, light-weight plastics with versatile properties tailored towards specific applications. The production of these petroleum-based plastics has increased considerably over the past few decades from about 1.65 million tonnes in 1950 [1] to 460 million tonnes in 2019 and its usage is expected to rise at a pace of 5% per year [2,3]. The extensive usage of these plastics (mostly single-use disposable) has, however, led to a huge generation of waste of about 353 million tons in 2019, with about 15% collected for recycling and only 9% being finally recycled [4]. This has led to serious global environmental problems such as increase in carbon footprint via waste combustion, and climate change issues whereby they emit greenhouse gases as they slowly decompose. Thus, the management of this waste, which involves their reduction, reuse, recycling, and recovering [5,6], is of paramount importance for minimizing the need for landfill. Thermoplastic polymers such as polypropylene (PP), polyethylene (PE), and polystyrene (PS) are the major components of municipal solid waste [7,8]. About 40% of this polymer waste comes from packaging, of which PS is a major component. Their use in packaging accounts for the global majority end-user market [9] and in most cases there is a short lifespan between their service and transformation. However, the majority of the collected waste is still being landfilled with the existing mechanical recycling and energy recovery processes not sufficient to deal with the ever-increasing plastic production and consumption [6]. Different processes can be utilized in the recycling of waste polymers to produce chemicals, liquid fuels, and hydrocarbon mixtures, such as pyrolysis, catalytic cracking and hydrocracking; and

* Corresponding authors.
E-mail addresses: olajumoke.alabi-babalola@manchester.ac.uk (O. Alabi-Babalola), carmine.dagostino@manchester.ac.uk (C. D'Agostino), arthur.garforth@manchester.ac.uk (A. Garforth).

https://doi.org/10.1016/j.fuproc.2025.108364
Received 10 July 2025; Received in revised form 29 October 2025; Accepted 11 November 2025
Available online 9 December 2025

understanding the structure-activity relationships in the catalytic conversion of waste is desirable [10].

Catalysis presents a valuable and sustainable tool to facilitate the selective conversion of plastic waste into valuable products under milder reaction conditions. Several catalytic strategies have been reported in literature towards the upcycling of plastic wastes [10–12], some of which involves their upgrading at the molecular level into high-value chemicals via depolymerisation and/or degradation. Strategies that have been reported in literature include: pyrolysis [7,8,13], catalytic pyrolysis [14–17], hydrogenolysis [18–20], hydrocracking [21,22], and oxidation [23–25]. Different researchers have also reported work on the recycling of PS, some of which include conversion into styrene over solid acids and bases [26–29], using supercritical solvents [30], conversion into polyelectrolytes [31], as well as conversion into different fractions of pyrolysis oil [32–34]. Current challenges involves the design and optimization of process conditions towards product selectivity [11], ensuring catalyst stability and the need to avoid catalyst poisoning towards real-life plastics processing. In the work reported herein, we focus on the catalytic hydrocracking of PS waste using cheap and sustainable bifunctional catalysts towards the selective production of the highly desirable liquefied petroleum gases and liquid ethylbenzene (EB). Catalytic hydrocracking in the presence of hydrogen helps in the removal of sulphur, nitrogen, and chlorine impurities to give products in the range of light to heavy hydrocarbons (diesel) with high amounts of isoparaffins and lower amounts of olefins [2]. It generally involves the use of a bifunctional catalyst with both metal and acidic functionality and a large surface area, typically a zeolite [35]. The hydrogenation is facilitated by the use of noble metals such as palladium or platinum, or by transition metals consisting of an alumina support loaded with cobalt, nickel, or molybdenum [36]. Selectivity and conversion are influenced by a number of factors such as the pore size of the zeolite, which affects mass transport between the molten viscous polymer and the zeolite structure, the acidity of the catalyst, as well as the operating reaction conditions.

The understanding of the adsorption of molecules in microporous zeolites helps in their design and applications for several industrial processes such as catalysis and separation [37]. The use of nuclear magnetic resonance (NMR) [38,39], amongst other methods such as infrared spectroscopy (IR) [40,41], temperature-programmed desorption (TPD) [42–44], and reactive gas chromatography [45], has been used to study adsorption and molecular dynamics in bulk fluids and fluids in porous systems in the last decade. NMR relaxation measurement is non-invasive and is an effective technique to probe guest-host molecular interactions of fluids in inorganic porous materials used for catalytic applications [37].

In our work, we compared different catalytic systems in the hydrocracking of expanded polystyrene (EPS) waste towards the selective production of liquid ethylbenzene. We synthesised Pt- and Ru-doped zeolite-based catalysts ($1Pt^0HY$, $1Ru^0HY$, $1Pt^0$ZSM-5) to introduce enhanced activity into the catalysts support. The structural and acidic properties were investigated, and the catalytic degradation of PS over the doped catalysts was carried out in a 300 mL stainless steel batch reactor in the presence of hydrogen. The effect of the synthesised catalysts on the thermal degradation of EPS waste were studied and the results showed that $1Pt^0HY$ and $1Ru^0HY$ showed high activity in converting EPS into ethylbenzene (EB), with selectivity being influenced by variation in reaction conditions. In addition, coke analysis was also carried out to determine the industrial suitability of the catalysts. We also carried out a comparative analysis of the effects of the parent zeolite, the calcined and reduced forms of Pt-doped HY with the key performance indicators being liquid conversion, EB product selectivity. The reusuability of $1Pt^0HY$ was further investigated for four repeated runs. Our target hydrocracking liquid product: (EB), is a valuable industrial feedstock used in the production of various synthetic products such as fuels, carpet glues, paints, inks, and insecticides. Therefore, providing an alternative route to its production can serve a variety of purposes, in addition to being a styrene monomer. It is currently produced from a liquid phase reaction between ethylene and benzene [46], the latter being a carcinogenic substance. The EB liquid selectivity is of great interest as it's current synthetic production route consumes about 50% of the world's production of benzene (a potential carcinogen), thus making finding an alternative production route an interesting and desirable area of interest in the petrochemical industry. In addition, the current market price of EB is approximately $1500 per ton [47], with a high volume of exports across Europe. Hence, replacing the current synthetic route via sustainable hydrocracking protocols appears promising and economical. This work aims to fully convert EPS into gas fractions (C_3 and C_4), liquid products (C_8-EB). We also propose a possible reaction pathway for the degradation of PS to ethylbenzene.

2. Methods

2.1. Feedstock and catalyst preparation

Tetraammineplatinum (II) chloride hydrate ($Pt(NH_3)_4Cl_2.xH_2O$) with a purity of 98% from Sigma Aldrich was used as the source of platinum. Powdered virgin polystyrene (VPS) of high purity with an average molecular weight of 192,000 g mol^{-1} was obtained from Sigma-Aldrich. The post-consumer EPS are from household waste and were crushed to an average particle size of 3.55 – 4.00 mm aperture **(Fig. S1)**. Platinum and Ruthenium (1 wt%) were loaded separately, via wet impregnation onto two zeolite supports: HY and ZSM-5 with a SiO_2: Al_2O_3 of 5 and 30 respectively which were obtained from Alfa Aesar. The metal salts ($Pt(NH_3)_4Cl_2.xH_2O$ and $RuCl_2.xH_2O$) were dissolved into 100 mL of deionized water at room temperature, and the resulting solutions were left to stir at 70 ℃ for about 8 h with a stirring speed of 500 rpm to ensure proper dispersion of the metal on the catalyst supports and gradual evaporation of water whilst forming a thick paste. The catalysts were oven-dried at 110 ℃ and the dried sample were calcined in a muffle furnace at 550 ℃ for 5 h at a ramp rate of 5 ℃ min^{-1} to allow decomposition of the metal salt [48]. Afterwards, they were converted to pellets of size 250–600 μm for subsequent reduction. Catalyst reduction was carried out using a tubular reactor by heating the catalyst pellets under a flow of hydrogen at a rate of 5 mL min^{-1} from ambient temperature to 400 ℃ at a flow rate of 10 ℃ min^{-1} for 4 h. Going forward and for ease of identification, the parent zeolites are designated as HY(5) and ZSM-5(30). The modified Pt-doped zeolites before hydrogen reduction are designated as 1Pt/Cal/HY and 1Pt/Cal/ZSM-5, and the reduced forms are $1Pt^0HY$ and $1Pt^0$ZSM-5 respectively. The calcined and reduced Ru-doped are designated as 1Ru/Cal/HY and $1Ru^0HY$ respectively.

2.2. Polymer and catalyst characterisation

The polymer feedstock was characterised via both thermogravimetric analysis (TGA) and Fourier transform infrared (FTIR). Catalysts characterisation was also performed using a range of methods including Pyridine-FTIR, Inductively coupled plasma optical electron spectroscopy (ICP-OES), BET nitrogen sorption isotherms, X-ray diffraction (XRD), ammonia-temperature programmed reduction (NH_3-TPD), and X-ray photoelectron spectroscopy (XPS). Other techniques include: the scanning transmission electron microscopy (STEM) and energy dispersive X-ray mapping which were acquired with a HAADF detector. In addition, NMR relaxation studies were also conducted on the HY catalysts carried out with a low-field carbon spinsolve Bruker DMX spectrometer. The details of the different analytical methods are supplied in the **Supplementary information (S1)**.

2.3. Hydrocracking reactions

Hydrocracking reactions were carried out using a 300 mL Parr reactor made of stainless steel, attached to an inlet stirrer [2]. The

feedstock polymer was mixed with catalyst with a specified polymer: catalyst ratio. The samples were loaded into the reactor, sealed, and purged using hydrogen gas, and subsequently charged to the reaction pressure of 20 bar H_2. The operating parameters to be varied for optimization were the reaction temperature (300–330 ℃), reaction time (15–90 min), reaction pressure (15–25 bar H_2), and polymer catalyst ratio (5:1, 10:1, 15:1). The desired reaction temperature was reached between 30 and 45 min, and subsequently kept isothermally constant for

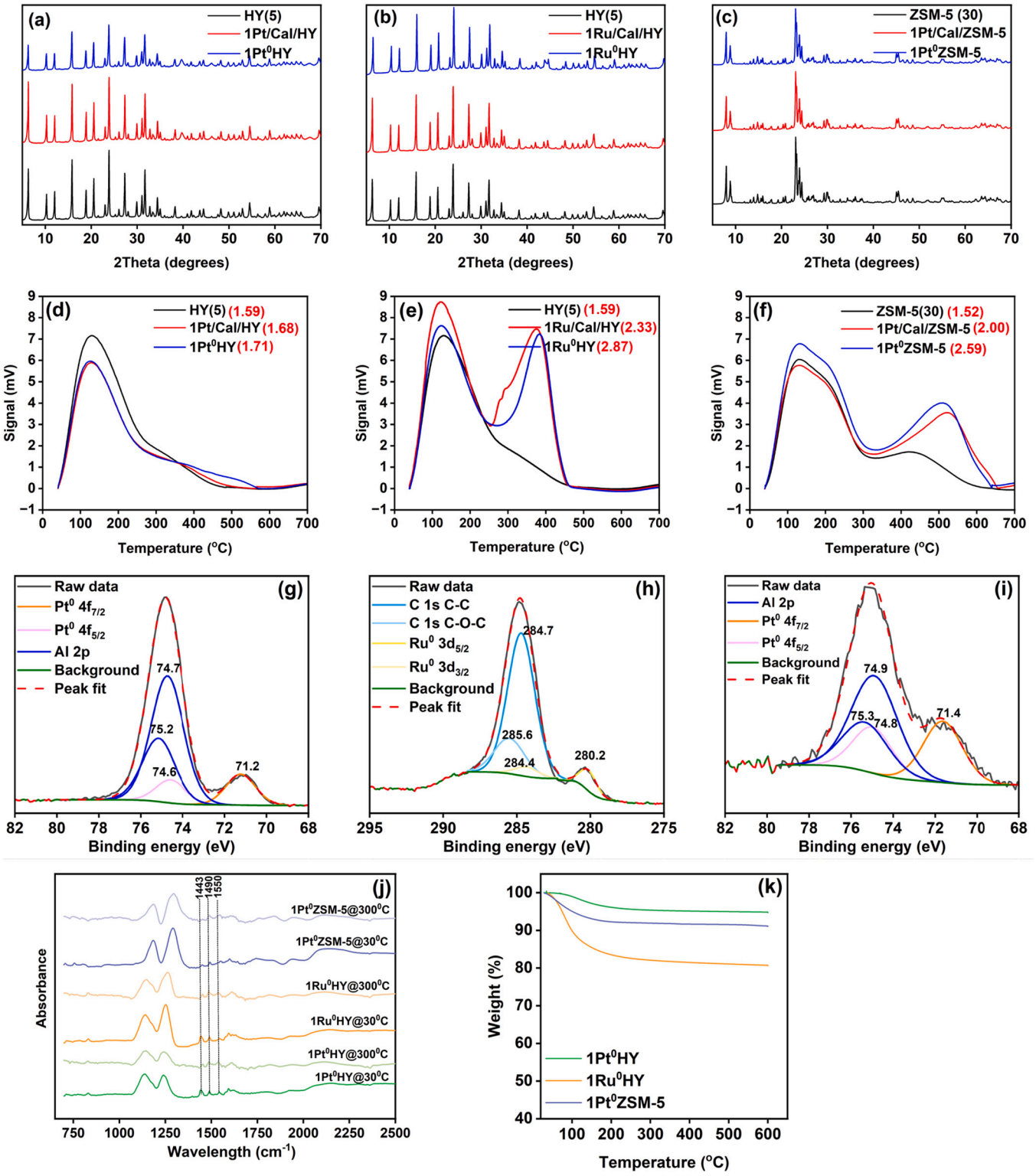

Fig. 1. Catalysts characterisation results: XRD patterns of parent and modified zeolite catalysts **(a)** HY(5) and Pt-doped HY **(b)** HY(5) and Ru-doped HY **(c)** ZSM-5 (30) and Pt-doped ZSM-5; NH_3-TPD desorption plots with acidity values (mmol/g of NH_3) in red parenthesis for **(d)** HY(5) and Pt-doped HY **(e)** HY(5) and Ru-doped HY **(f)** ZSM-5(30) and Pt-doped ZSM-5; XPS peak deconvolution of **(g)** Al 2p and Pt 4f spectra for $1Pt^0HY$ **(h)** C 1s and Ru 3d spectra in $1Ru^0HY$ **(i)** Al 2p and Pt 4f spectra for $1Pt^0ZSM5$ **(j)** Pyridine-FTIR desorption analysis of synthesised catalysts at 30 and 300 ℃ **(k)** TGA analysis of fresh synthesised catalysts. (For interpretation of the references to colour in this figure legend, the reader is referred to the web version of this article.)

the desired reaction time with constant agitation of 400 ± 15 rpm. At the end of the reaction, the reactor was allowed to cool to ambient temperature, and the hydrocracking products were collected for further analysis.

Gas products were analysed using a Varian CP 3800 gas chromatography (GC) attached to a 50 m × 0.32 mm i.d. PLOT Al_2O_3/KCl capilliary column and a flame ionization detector (FID) with the hydrogen concentration present in the gas stream being measured with a mass spectrophotometer (MS) (Hiden Analytical). The liquid products were analysed using an Agilent Technologies 6890 N Network GC–MS fitted with a 100m × 0.25 i.d. PONA CB column. The catalysts were reused for four repeated runs using the conditions: 330 ℃, 20 bar H_2, and 60 min, with an initial polymer : catalyst ratio of 10:1. At the end of the reaction, the product liquid was filtered, reactor dried, and the coke residue was obtained, followed by further hydrocracking reactions. Coke analysis of some spent catalysts was carried out via TGA.

3. Results and discussion

3.1. Polymer and catalysts analysis

The thermal degradation profiles of both EPS and VPS at different heating rates (5–20 ℃ min^{-1}) are shown in **Fig. S2**. There are three major degradation steps: drying, devolatilization (decomposition), and char formation. In the drying zone, there was negligible weight loss up to 330 ℃ implying that the molten polymer was thermally stable up to this temperature with negligible moisture. The single-step decomposition stage occurred between 300 ℃ and 460 ℃ whereby there is evaporation of both light and heavy organic carbonaceous compounds and about 95% of PS solid matrix has decomposed. As the heating rate of the polymer increases from 5 to 20 ℃ min^{-1}, the onset and maximum decomposition temperatures increase from 428 ℃ at 5 ℃ min^{-1} to 460 ℃ at 20 ℃ min^{-1}, which is consistent with data reported in the literature [49–53]. The difference in the degradation temperatures at different heating rates is due to kinetic or heat transfer limitations associated with continued weight loss as the molten polymer decomposes. The third stage is the char formation occurring at temperatures above 460 ℃, containing the carbon residue at constant weight. The difference in conversion for both VPS (100%) and EPS (97%) is attributed to the nature and molecular weights of the feedstock. In addition, the observed weight loss is an indication that the thermal degradation of PS in the presence of a non-inert atmosphere will exhibit a reductive behaviour [51].

The activation energy E_a was obtained using the Flynn-Wall-Ozawa's (FWO) method [54–57] at different degrees of conversion from the slope of the plots of logarithm of heating rate (β) against $1/T$. As temperature increases, conversion also increases at a constant heating rate, and the activation energies were obtained to be in the range of 179–184 kJ mol^{-1} and 180–186 kJ mol^{-1} for VPS and EPS respectively, which agrees with values reported in literature [58].

Catalysts characterisation results are shown in Figs. 1a-i**.** XRD patterns of both parent and modified HY confirmed the structure of the materials [59–61], with Pt diffraction peaks displayed at $2\theta = 40^{\circ}$ and 46° for the Pt-doped catalysts [62] implying that the Pt molecules are effectively supported on the modified zeolites. The structural ordering of the doped catalysts is maintained despite the heat treatment as seen in Figs. 1a-c, implying that the structure has not been damaged by both metal impregnation and heat treatment.

On the other hand, the absence of Ru peaks (see Fig. 1b**)** often located at 2θ of 38.4, 42.2, and 44° which corresponds to (100), (002), and (101) planes [63] indicates a well dispersed ruthenium on the zeolite surface. The crystallinity of these zeolites were calculated in the 2θ range of 5–55° **(Eq. 1)** and results show a slight decrease in crystallinity after Pt impregnation with values of 39, 35, and 31% for HY(5), 1Pt/Cal//HY, $1Pt^0$HY respectively. The Ru-doped catalysts decreased in crystallinity values from 39% (HY(5)) to 34 (1Ru/Cal/HY), and 31% ($1Ru^0$HY). However, the crystallinity of Pt-doped ZSM-5 catalysts has remained relatively the same at 38% following the addition of platinum.

$$Crystallinity\ (\%) = \frac{Peak\ area\ of\ eight\ most\ intense\ peaks}{Total\ peak\ area\ between\ 5-55^{\circ}} \quad (1)$$

NH_3-TPD measurements showed different peaks associated with the acid and metal sites (Fig. 1d-f**)**. The peaks at the low temperature region 100–300 ℃ are attributed to weakly adsorbed ammonia, while the peaks at the high temperature region 350–600 ℃ are the strong acid and metal sites [43], which usually plays the active role in catalytic reactions [64]. There is a decrease in the number of weak acid sites (with maxima at 124 ℃) for the Pt-doped HY catalysts **(Fig. 1d)** which can be attributed to the reduction in the extra-framework penta-Al species (dealumination) upon Pt-doping resulting in the reduction of the Si-OH-Al concentration. In addition, the thermal treatment may likely replace the H^+ in both silanol (Si-OH) and Si-Al-OH groups leading to a decrease in concentration of the hydroxyl groups, and thus lower number of acid sites [65]. The acidity of the Ru-doped HY catalysts (Fig. 1e**)** and Pt-doped ZSM-5 (Fig. 1f**)** has increased following introduction of the metal crystallites resulting in a more intense maxima in the high temperature regions at 378 and 515 ℃ respectively. The total acidity values and surface properties of the catalysts are shown in **Table S1.** The total acidity of the bifunctional catalysts increased as a result of the introduction of metal species on the catalyst surface which created new acid sites in the high temperature region of the thermograms. At relatively low loadings (1%), the transition metals are widely dispersed, interacting strongly with the zeolite framework to form metal cations thereby introducing more Lewis acidity, and producing a cumulative effect on the total acidity.

We investigated the effect of Pt doping and reduction on the HY catalysts using XPS. The deconvolution of the C 1s spectra of the HY catalysts showed identical peaks at 284.8, 285.9, and 289.3 eV **(Table S2, Fig. S3)** corresponding to the energy states of C—C, C—O, and C═O respectively [66]. There are no significant changes to the C 1s peaks upon Pt metal deposition. Al 2p analysis shows the appearance of a new chemical environment after the introduction of platinum **(Fig. S5a-c)**. There is an overlap between Al 2p and Pt $4f_{7/2}$ energy states [67] and the binding energies are obtained by fitting the overlapping regions.

The Al $2p_{3/2}$ and $2p_{1/2}$ peaks of HY(5) are located at 75.0 and 75.44 eV, respectively, with a doublet splitting of 0.44 eV corresponding to differently coordinated aluminium states (AlOH) in the zeolite framework [68,69]. There is a change in the Al 2p energy states for the Pt-doped catalysts with a decrease of 0.1 eV (1Pt/Cal/HY) and 0.3 eV ($1Pt^0$HY) for $2p_{3/2}$ **(Table S3)** strongly suggesting a decrease in their alumina content and a possible shortening of the average Al—O bond [70,71] as a result of thermal treatment of the catalysts.

The survey spectra for $1Pt^0$HY, $1Ru^0$HY, and $1Pt^0$ZSM-5 are shown in **Fig. S4a-c**, and the peak deconvolution showing the respective oxidation states of the metals are highlighted in Fig. 1g-i and BE values shown in **Table S4.** The fitting of the Pt 4f profiles were subject to the constraints Pt (4f) doublet separation (≈3.35 eV) and an intensity ratio Pt ($4f_{5/2}$)/ Pt ($4f_{7/2}$) as 0.75 [72,73] **(Figs. S5b,c, 1 g,i)**. The peak at 71.4 eV for 1Pt/Cal/HY **(Fig. S5b)** indicates the presence of Pt $4f_{7/2}$ electrons. However, this is higher than that of bulk Pt metal (71.0 eV) [69,74] by approximately 0.4 eV suggesting the presence of the formation of Pt_2Si or a proton at this energy level due to the thermal decomposition of the Pt tetraamine ions prior to hydrogen reduction in which the decomposition of the complex ions is expected to alter the symmetry and the Pt zeolitic environments. The binding energy of Pt $4f_{7/2}$ at 73.8 eV confirms the presence of PtO with the metal having an oxidation state of 2+ [67,75]. Pt $4f_{7/2}$ and $4f_{5/2}$ profiles for $1Pt^0$HY (Fig. 1g) showed the asymmetric doublet splitting at 71.2 and at 74.6 eV respectively which corresponds to the energy level of Pt metal [76]. Similarly, Pt metal 4f peaks were observed for $1Pt^0$ZSM-5 with an overlap with Al 2p (Fig. 1i) with the higher and lower energy levels observed at 71.4 and 74.8 eV **(Table S4)** respectively. The Ru 3d peaks

often overlaps with C 1s [77] and the peak deconvolution as shown in Fig. 1h confirms the presence of Ru metal in $1Ru^0HY$. The binding energies of the two asymmetric Ru 3d peaks: Ru $3d_{5/2}$ and $3d_{3/2}$ are obtained at binding energies of 280.2 and 284.4 eV and agrees with values obtained from literature for Ru metal with a split spin-orbit spacing of 4.2 eV [78].

The Pyridine-FTIR analysis **(**Fig. 1j**)** revealed both Brønsted acid sites (BAS) and Lewis acid sites (LAS) at 1540 and 1443 cm^{-1} respectively [79,80], with the LAS more pronounced as a result of metal impregnation which increased the total acidity as seen in the TPD analysis **(**Fig. 1d-f**).** There is also a peak at 1490 cm^{-1} which corresponds to both acids sites as a result of overlapping. The pyridinium ion (PyH^+) at 1540 cm^{-1} is formed when the BAS reacts with pyridine via protonation, while the band assigned to LAS is formed as a result of pyridine coordinated to LAS (extra framework aluminium) through a dative bond [81]. The TGA analysis **(**Fig. 1k**)** showed thermally stable catalysts at high temperatures of up to 600 ℃, after the removal of moisture (at temperatures below 100 ℃).

HAADF-STEM images for the reduced catalysts are shown in Figs. 2-**c**; and their respective average particle sizes obtained as 10.3, 13.1, and 2.5 nm (**Figure 2di-iii)**. The elemental mappings further confirm the presence of the silica-alumina (Si, O, Al) contents as well as the presence of the metal crystallites on the zeolite.

The BET nitrogen adsorption-desorption isotherm showed an increase in the isotherm at low P/P^o **(Fig. S6)** with the hysteresis loop at about $P/P^o \sim 0.45$ for the synthesised catalysts, indicating a potential presence of mesopores generated by dealumination during the impregnation process [2]. The presence of the metal crystallites on the catalyst support led to a decrease in the surface area **(Table S1)** because the impregnation process resulted in the reduction of the Si-OH-Al groups. The BET surface area of the bifunctional catalysts was obtained as 536, 438, and 312 $m^2\ g^{-1}$ for $1Pt^0HY$, $1Ru^0HY$, and $1Pt^0ZSM\text{-}5$ respectively.

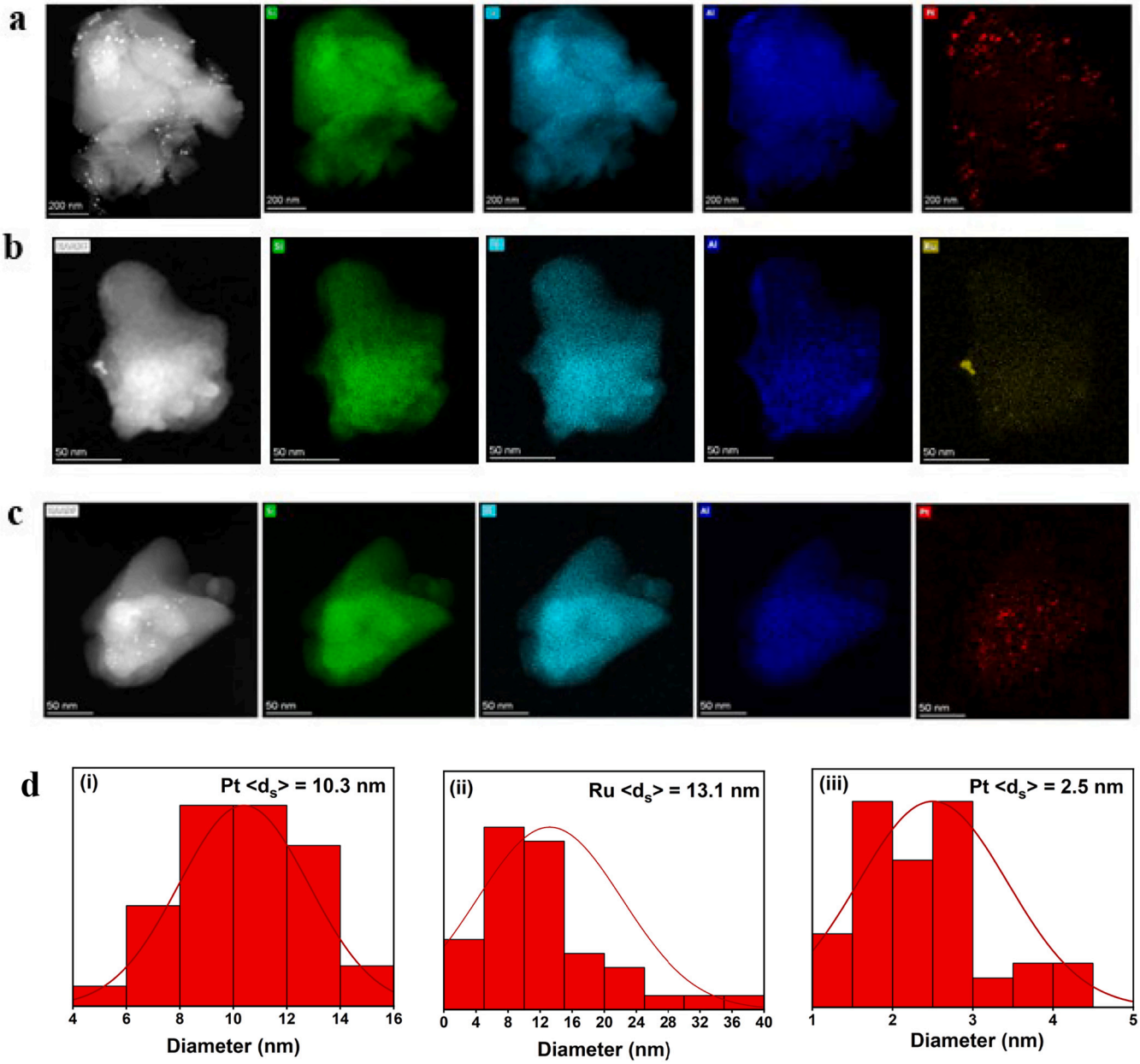

Fig. 2. a. STEM/EDX elemental mapping for Si, O, Al, and Pt of $1Pt^0HY$ catalyst. **b.** STEM/EDX elemental mapping for Si, O, Al, and Pt of $1Ru^0HY$ catalyst. **c.** STEM/EDX elemental mapping for Si, O, Al, and Pt of $1Pt^0ZSM\text{-}5$ catalyst. **d.** (i) Pt particle size distribution for $1Pt^0HY$ catalyst (ii) $1Pt^0ZSM\text{-}5$ (iii) Ru particle size distribution for $1Ru^0HY$ (c). Symbol $\mathbf{<d_s>}$ denotes the average particle size of platinum (nm).

The Dubinin-Radushkevich average pore diameter of $1Pt^0HY$ was 0.6 nm and that of $1Ru^0HY$ was 0.7 nm, thus indicating that the addition of Ru on HY(5) further increased the average pore size of the synthesised catalyst. However, the pore diameter of $1Pt^0ZSM\text{-}5$ was significantly higher (3.89 nm) implying that ZSM-5 has larger pore size [82] compared to the HY. The micropore volumes obtained for the catalysts all fall within the range of values reported in literature [82–86]. The ICP-OES analysis of the catalysts revealed 0.97% Pt, 0.91% Ru and 0.94% Pt for $1Pt^0HY$, $1Ru^0HY$, and $1Pt^0ZSM\text{-}5$ respectively. These obtained ICP-OES values agree with the experimental amounts, implying the catalysts were prepared accurately.

3.2. Hydrocracking reactions

The hydrocracking of EPS produces gaseous, liquid, and coke residue. During reaction, the EPS polymer chains break into the molten state via either end-of chain scissions or random scissions of the polymer chains [9]. These effects lead to a simultaneous decrease in the molecular weight of the unconverted polymer, followed by conversion to various products. The amount and nature of each product depends on the reaction conditions. Generally, gas products of EPS ranges from C_1–C_9 with negligible amounts of olefinic content. The major gas products were the liquefied petroleum gases (LPG): C_3H_6 and C_4H_{10}. The liquid products for Pt-doped HY are mainly aromatics (denoted as A in our work) namely A_6-benzene, A_7-toluene, and A_8- ethylbenzene (EB), *p*-xylene (PX), *m*-xylene (MX), and *o*-xylene (OX). A_9, A_{10}, and A_{11} are aromatics with 9, 10, and 11 carbon numbers respectively; and are mainly derivatives of benzene in which the aromatic ring is attached to an alkyl substituent. The cycloalkanes (denoted as C_y) consist mainly of C_{y6}–C_{y10}, comprising cyclohexane and its alkyl derivatives. Other liquid products include paraffins (butane, pentane and related compounds), indanes, naphthalenes, and polyaromatics (PAHs). The amount of each component in the liquid stream largely depends on mass transfer resistance associated with varying reaction conditions of temperature, time, pressure, polymer:catalyst ratio, as well as the reusability of the catalysts.

Prior to hydrocracking, preliminary reactions on thermal cracking of both EPS and VPS with no catalyst and it was observed that there was no selectivity in the distribution of products. In addition, the gas products contain a lot of unsaturated olefins (C_2, C_5–C_9), while the liquid products contain higher amounts of the diesel-range heavy molecular weight hydrocarbons and polyaromatics.

3.2.1. Effect of reaction time on hydrocracking reactions of Ru-doped and Pt-doped catalysts

Time-dependent hydrocracking reactions between 15 and 90 min were carried out to investigate the effect of contact time between the molten polymer and the synthesised bifunctional catalysts: $1Pt^0HY$, $1Ru^0HY$, and $1Pt^0ZSM\text{-}5$ on conversion and product selectivity (Table 1, Fig. 3a-h). There is a progressing transition from solid to fluid with almost complete conversion at 90 min for the HY-doped catalysts. Interestingly, there are approximately no liquid products obtained for $1Pt^0ZSM\text{-}5$ reactions with the gas yield accounting for over 90% of the hydrocracking products, which is largely attributed to its relatively large pore size of 3.8 nm **(Table S1)** and smaller channels [87,88] which promotes fast mass transport and reducing the possibility of secondary reactions [89].

The volatile alkanes ($C_2 - C_4$) are the predominant gas products for $1Pt^0ZSM\text{-}5$ (Fig. 3c), with C_2 (23 – 27 %), C_3 (52 – 54 %), and C_4 (14 – 17 %) at different reaction times. Interestingly, $1Pt^0ZSM\text{-}5$ have higher selectivity towards C_2 alkane compared to both $1Pt^0HY$ and $1Ru^0HY$ (Fig. 3a and b), which can be attributed to the nature of its framework [90], and probably due to its much lower average Pt particle size of 2.5 nm as obtained from STEM analysis.

It was also observed that the total gas yield was found to slightly increase with time for Pt-doped reactions but decreased with time for Ru-doped reactions. In addition, Ru was more selective towards C_3 (61% at 90 min) compared to Pt (34% at 90 min), on the same support- HY(5). Generally, the presence of the metal active sites promoted catalytic reactivity allowing formation of smaller cracked molecules.

The liquid product distribution by carbon number is shown in **Figs. S7a-b.** The liquid product distribution by selectivity revealed a peak of 69% of single-ring aromatics for $1Pt^0HY$-catalysed reaction at 15 min. However, at 90 min reaction time, this amount decreased to 40% leading to a corresponding increase in the number of naphthenes i.e. cycloalkanes (45%) (Fig. 3d). This strongly indicates that longer reaction times promoted the hydrogenation of the aromatic rings of both benzene and EB molecule as observed in C_{y6} and C_{y8} (Figs. 3e, g), suggesting the possibility of an equilibrium shift towards de-aromatisation at the active catalytic sites [86,91] likely due to its higher number of pore volumes 0.33 $cm^3\ g^{-1}$ (mesopores 0.08 $cm^3\ g^{-1}$) which become more easily accessible at longer reaction times.

For $1Ru^0HY$-catalysed reactions, the predominant liquid products are the single-ring aromatics (Fig. 3f), with EB accounting for 38 – 43% (Fig. 3h), which is slightly higher than those of $1Pt^0HY$ reactions (17 – 37 %), which could be attributed to the more acidic nature of $1Ru^0HY$ as discussed in the TPD analysis. In addition, at 90 min reaction time, while de-aromatisation occurred for $1Pt^0HY$ reactions, the mechanism of $1Ru^0HY$ remained the same, implying more catalyst stability of the latter. These results also indicate that at higher reaction times, hydrogen transfer reactions involving dehydrogenation of fused ring aromatics into single ring aromatics becomes predominant for $1Pt^0HY$ reactions, and that Ru showed enhanced selectivity and stability towards EB molecule compared to Pt.

It is interesting to note that EB is the major hydrocracked liquid product accounting for ~92% of A_8 fraction, with the remainder (<8 %) being the isomers of xylenes. The absence of styrene in the liquid product stream was due to the presence of hydrogen, which serves as an inhibitor in chain unzipping reactions of PS depolymerisation; thus, expelling styrene monomers [91]. Several authors [2,9,26,91–95] have reported the chemical upcycling of PS via several reaction protocols such as pyrolysis [95] and hydrocracking [9,96]. However, most of the results reported often requires higher pressure or temperature, longer contact times and no selectivity towards specific products. Fuentes-Ordóñez et al. [92] in their work in the catalytic hydrocracking of polystyrene in solution on Pt/H-Beta catalyst reported their major liquid products as isoparaffins and naphthenics [9]. González-Marcos et al. [9] in their use of different bifunctional Pt-supported Al_2O_3, HY, HBeta, and HZSM-5 catalysts in PS hydrocracking reported the production of gasoline fractions and aromatics at temperatures between 325 – 425 °C and 18 MPa hydrogen. The more concentrated C_8 molecules which are preferentially formed in the liquid stream are as a result of the higher amount of Lewis acidity, which occurs as a direct consequence of the introduction of active metal sites on the catalytic surface.

Table 1
Conversion values (%) for time-dependent hydrocracking reactions of Ru-doped and Pt-doped zeolite catalysts.

Catalysts	15 min			30 min			60 min			90 min		
	Gas	Liquid	Solid	Gas	Liquid	Solid	Gas	Liquid	Solid	Gas	Liquid	Solid
$1Pt^0HY$	24	39	37	30	63	7	30	67	3	29	71	0
$1Ru^0HY$	42	52	6	27	70	3	27	70	3	22	76	2
$1Pt^0ZSM\text{-}5$	93	3	4	94	2	4	96	–	4			

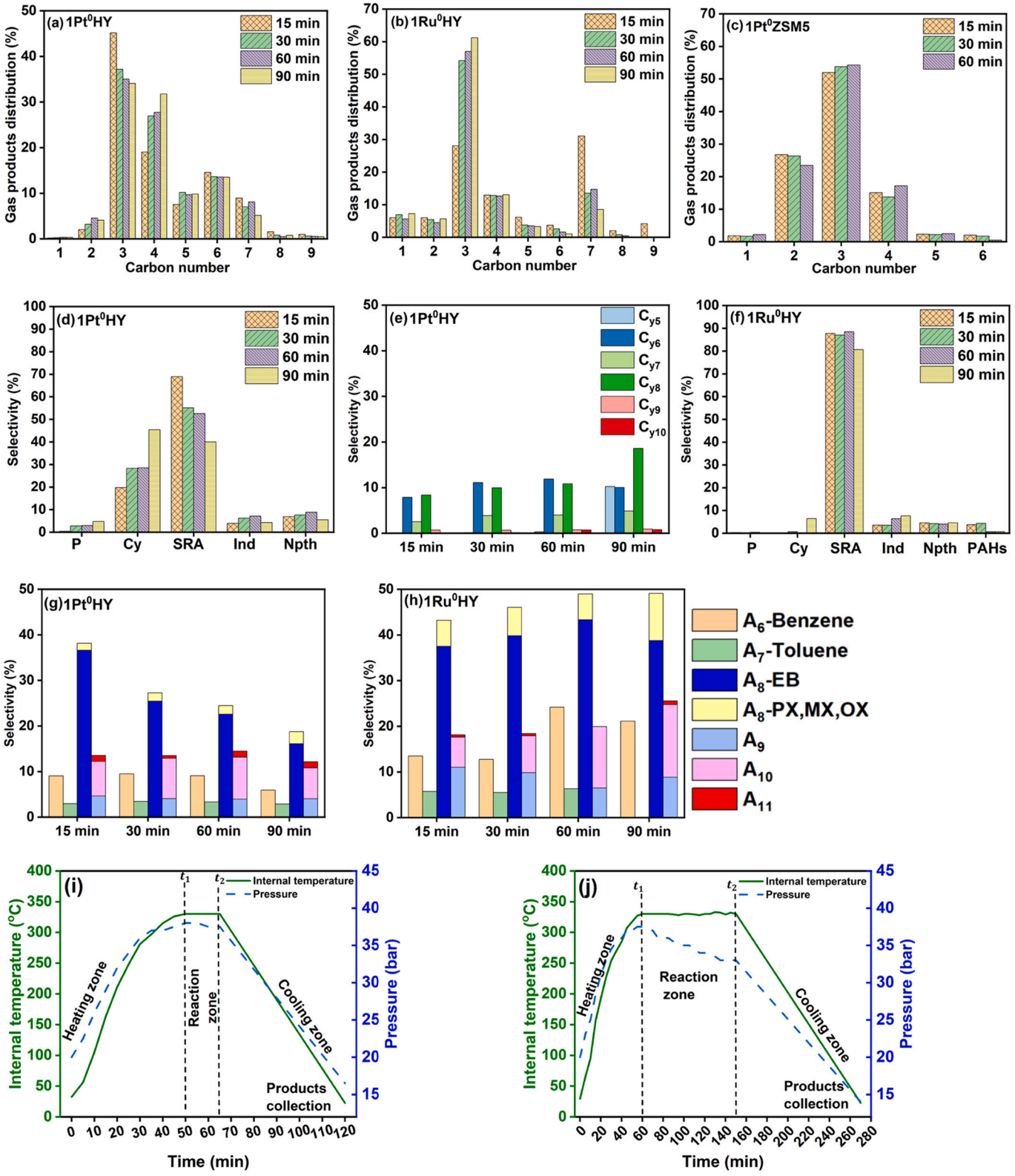

Fig. 3. Product distribution for time-dependent EPS hydrocracking reactions at 330 °C, 20 bar H_2, 10:1 polymer: catalyst ratio; Gas products analysis for **(a)** $1Pt^0HY$ **(b)** $1Ru^0HY$ **(c)** $1Pt^0ZSM$-5; **(d)** Liquid selectivity for $1Pt^0HY$ **(e)** Cycloalkane selectivity for $1Pt^0HY$ **(f)** Liquid selectivity for $1Ru^0HY$ **(g)** Single-ring aromatic distribution for $1Pt^0HY$ **(h)** Single-ring aromatic distribution for $1Ru^0HY$; Typical temperature-pressure profiles for PS hydrocracking over $1Pt^0HY$ catalyst at 330 °C, 10:1 polymer:catalyst ratio, 20 bar H_2 at different reaction times **(i)** 15 min **(j)** 90 min; t_1 and t_2 represents start and end of agitation respectively, with an observed pressure drop immediately after t_1. **Key:** P-Paraffins, Cy-Cycloalkanes, SRA-Single-ring aromatics, Ind-Indanes, Npth-Naphthalene, PAHs-Polyaromatic hydrocarbons.

During PS degradation, benzene is often formed at the BAS of the bifunctional catalysts [92] when a proton is added to the electron-rich phenyl group to form an intermediate carbenium ion which further degrades the C—C bond linking the chain with the phenyl group via β-scission, to produce a second carbenium ion and benzene. On the other hand, C_8 molecules are formed over the LAS [96] at high reaction temperatures [91,94], whereby the LAS accept electrons from the alkyl-terminated saturated chain ends of the polymer molecule to produce carbenium ions which are further protonated to C_8 molecules. However, the formation of EB, rather than the unsaturated styrene molecule was due to hydrogenation of the ethylene substituent which is attributed to the presence of the active metal site. The cycloalkanes were also formed via hydrogen transfer reactions whereby isoparaffins are converted into cyclic compounds. This occurs when the alkyl substituent of the isoparaffins acts as hydrogen donors, generating carbocations in situ acting as hydrogen acceptors [97]. This leads to the formation of a scaffold in which the carbocation is subjected to a cyclization reaction forming naphthenes (cycloalkanes) [91].

The temperature and pressure profiles for reactions occurring at 15 and 90 min are shown in Figs. 3i,j highlighting three different zones: heating, reaction, and cooling zones. The heating zone increases linearly with time as heating progresses, while the reaction zone is an isothermal process (330±3°C) which occurs during the agitation period (between t_1 and t_2), with a slight pressure drop. Both temperature and pressure decrease linearly with time in the cooling zone.

3.2.2. Effect of reaction pressure and polymer : catalyst ratio

Increasing hydrogen pressure from 15 to 25 bar significantly enhanced degradation of PS promoting $X_{solid \rightarrow fluid}$ conversion from 37 to 73% at just 15 min of reaction time **(Fig. S8a).** Hydrogen solubility is expected to increase with pressure [98], thereby enhancing diffusion and mixing between the polymer and catalyst leading to increasing activity between catalyst and product molecules [2]. At low pressure of 15 bar H_2, there was still small amounts of naphthalenes and PAHs **(Fig. S8b)** implying insufficient hydrogenation, while at higher pressures of 25 bar, saturated ring-opening products are preferentially produced. Variation in catalyst loading relative to amount of polymer was found to have negligible effect on conversion, but significant effect on product selectivity **(Fig. S8c)**. Higher amounts of lower molecular weight liquid paraffins (15%) and cycloalkanes (34%) were preferentially produced at 5:1 than at 15:1: paraffins (1%), cycloalkanes (12%). This can be explained away by the fact that high amounts of catalysts increased the number of active metal sites responsible for hydrogenation reactions leading to more saturated and ring opening products [99] consisting of paraffins and isoparaffins. Conversely, lower catalyst loading (15:1) gave more aromatics (68%) than at reaction involving 5:1 (44%).

Thus, reaction pressure was found to significantly affect yield and conversion, while EB selectivity and product distribution are largely dependent on reaction time and the polymer:catalyst ratio. Thus, we can infer from the results obtained that for optimum PS conversion and EB selectivity, the optimum reaction time, pressure and polymer:catalyst ratio should be 15 min, 20 bar H_2, and 10:1, respectively.

3.2.3. Coke analysis

The thermal degradation profiles of the bifunctional catalysts used in EPS hydrocracking are shown in Fig. 4a-c at different heating regimes from ambient to 600 °C. The amount of coke formed was obtained as the weight difference when the system is switched from nitrogen to air at 600 °C. Coke production increased with increasing reaction time for $1Pt^0HY$: 7, 8, 14, and 14% at 15, 30, 60, and 90 min respectively **(**Fig. 4a**)**. However, the amount of coke for $1Ru^0HY$ were between 11 – 12% **(**Fig. 4b**)**, while those of $1Pt^0ZSM$-5 were between 3 – 4% **(**Fig. 4c**)** and found to be independent of reaction time**.**

The difference in the amounts of coke formed for the different catalysts is due to the nature of their acid sites, and their extent of porosity. The higher mesopore volumes (0.08 $cm^3\ g^{-1}$) of the less acidic $1Pt^0HY$ as obtained from BET Analysis **(Table S1)** facilitates coke formation and also agrees with results reported by Fals et al. [100]. Also, the presence of larger pores for $1Pt^0ZSM$-5 (3.8 nm) favours more chain cracking reactions resulting in lower adsorption of coke precursor species.

3.3. Proposed mechanism for production of ethylbenzene from PS

The mechanism of PS degradation follows three (3) steps: initiation, propagation, and termination. The degradation steps and subsequent products formed depends on the cracking conditions, nature and type of catalyst, such as the presence of metallic and acidic centres on the catalyst surface [96]. The initiation process of PS degradation involves the breaking of C—C bonds, or C—H bond fission to form free radicals; propagation involves different hydrogen transfer or β-scission reactions to produce oligomers (monomers, dimers, and trimers). It is important to note that most bond scissions occur on the zeolite surface sites so that the hydrocarbon of similar sizes can enter the pores to achieve potential selectivity. The termination step include recombination, disproportionation, and radical addition reactions [91,101]. Several mechanisms have been proposed for acid-catalysed degradation of PS [92,102] with the first step being an initiation step involving an electrophilic proton attack on either the ortho- or para- position of the aromatic ring leading to the formation of a carbenium ion, a saturated chain end or a chain end cation [102]. This is followed by a series of propagation reactions involving chain shortening via β-scissions, inter- or intra-molecular hydrogen transfer reactions, hydride abstraction, proton rearrangement, or cyclization reactions to form different degradation products such as paraffins, olefins, alkyl benzenes, indane, indenes, naphthalene's, and polyaromatics. The nature and abundance of products formed depends on the predominant decomposition pathway which is largely influenced by the volume of the zeolite channel. The termination steps often involve combination reactions between the carbenium ions and the free radicals or disproportionation reactions, leading to the formation of coke.

The initiation begins with an electrophilic attack at the ortho- position of the polymer molecule by protons which leads to the formation of

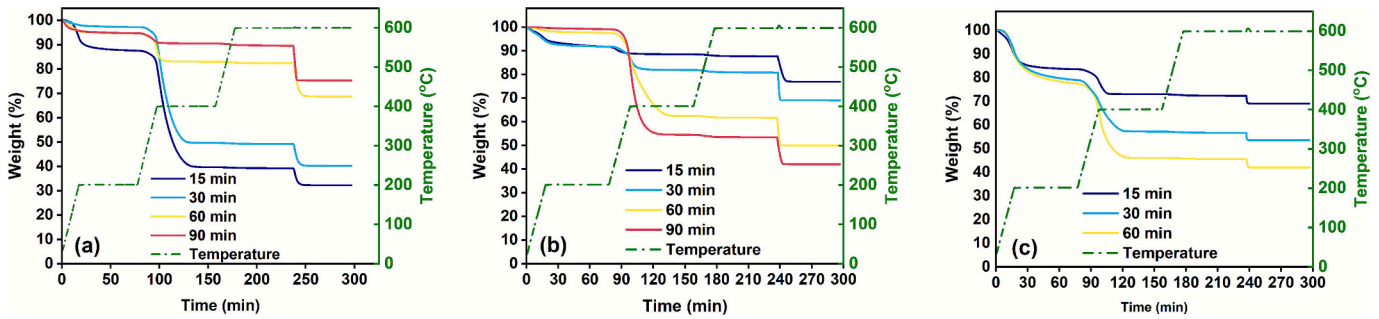

Fig. 4. Thermal degradation profile of spent bifunctional catalysts in the hydrocracking reactions of EPS (a) $1Pt^0HY$ (b) $1Ru^0HY$ (c)$1Pt^0ZSM$-5.

a chain end cation and a methyl-terminated saturated chain end (Fig. 5a).

We propose three different possible propagation mechanisms in the formation of ethylbenzene (Fig. 5b) whereby the initiation products are involved in a series of transformation reactions. The chain end cation **(1)** can further decompose to form a smaller carbocation and an unsaturated chain end which could be styrene. The produced styrene molecule then undergoes hydrogenation in the presence of metal catalysts leading to the formation of ethylbenzene. The second involves the protonation of the methyl-terminated chain end, followed by decomposition and hydrogenation reactions **(2)**. The third pathway is the protonation of the aromatic ring located at the styrene-terminated chain ends, subsequently followed by decomposition leading to the formation of ethylbenzene **(3)**.

3.4. Catalysts reusability reactions

The $1Pt^0HY$ catalyst was tested for its reusability using four repeat experiments at 330 °C, 60 min, and 20 bar H_2 pressure. The catalysts were separated from the reactions by filtration, followed by direct evaporation. Fig. 6a shows the overall yields of the different repeat runs with a slight increase in the liquid extract after each run. The increased liquid yield could likely be due to the initial deposition of the heavier cracked molecules on the catalyst's surface, thus altering the pore structure and increasing the surface area for further cracking of the larger molecules during subsequent hydrocracking reactions. Identical result was also reported by García et al. [103] in their use of a liquid catalyst in the hydrocracking of heavy oil. The gas product distribution (Fig. 6b) showed a decrease in C_3 molecules and a decrease in the iC_4: nC_4 ratio confirming a reduction in isomerization, and probably a decrease in catalyst activity. There was also the increasing presence of C_7= molecules due to decreased level of saturation associated with the reduced hydrogenation function of the metal support. The quality of the liquid oil obtained was different as it gradually turned into pyrolysis oil as the number of repeated runs increases. Liquid products distribution (Fig. 6c) revealed a decrease in C_6 which was predominantly benzene, suggesting a decrease in BAS of the reused catalyst [96]. Also, a steady increase in PAHs ($C_{13}C_{16}$) confirmed a reduction in both acid and active

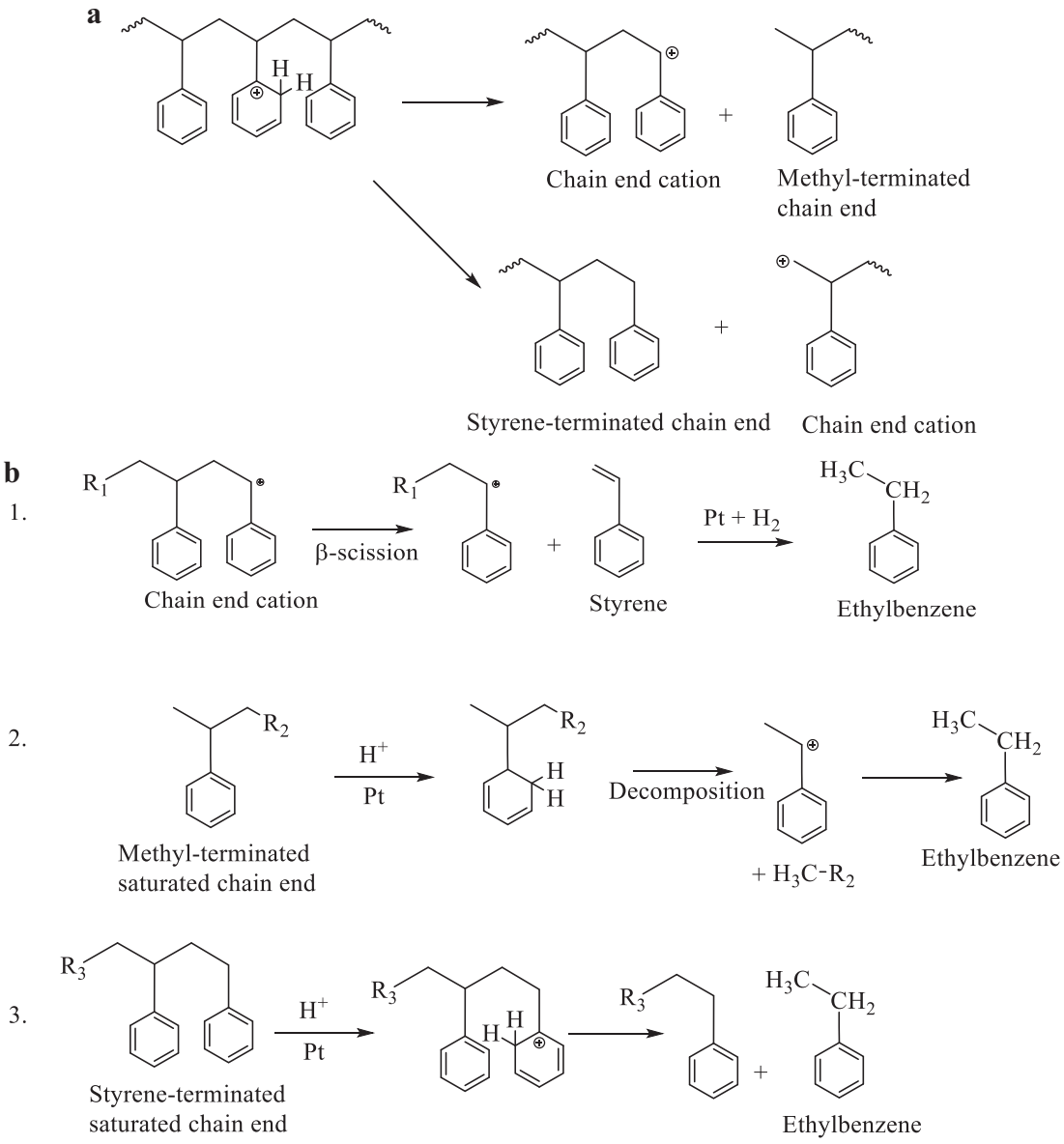

Fig. 5. a. Initiation mechanism via β-scission for PS degradation towards formation of ethylbenzene, modified from [102]. **b.** Proposed propagation steps in the production of ethylbenzene.

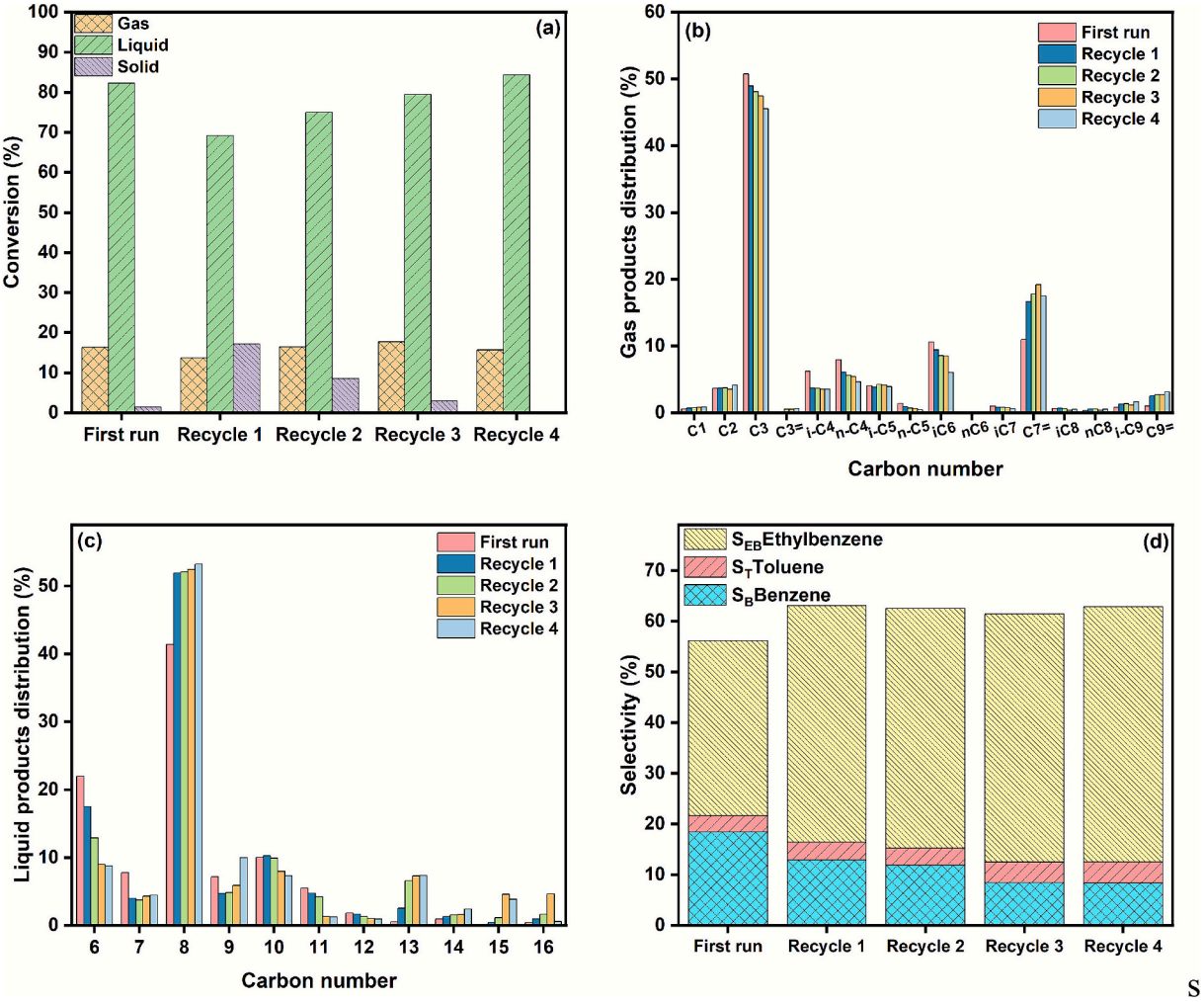

Fig. 6. Reuse of $1Pt^0HY$ catalyst for EPS hydrocracking at 330 °C, 20 bar H_2 gas showing (a) Yield (b) Gas products distribution (c) Liquid products distribution (d) Selectivity.

metal sites since these sites are responsible for cracking and hydrogenation reactions respectively. Interestingly, this was not the case with C_8 molecules, which shows an increase in C_8 (predominately EB) with repeated runs; suggesting that the Lewis acid centres [9] remain relatively unchanged. The similar selectivity of $1Pt^0HY$ towards EB (Fig. 6d) after four repeated cycles is a good indication that the catalysts can be regenerated and reused after evaporation for series of repeated experiments. It also indicates that the catalyst is thermally stable with a good resistance towards sintering.

3.5. NMR relaxation studies

NMR relaxation T_1/T_2 studies of both parent and modified catalysts were carried out to understand the molecular dynamics and surface interactions of different probe molecules in the cavity of the zeolite framework. Eight different probe molecules consisting of ethylbenzene, *p*-xylene, *m*-xylene, *o*-xylene, water, cyclohexane, *n*-octane, and squalene were used to obtain relaxation plots for the studied catalysts. Within the zeolite framework, the observed relaxation times depends on surface interactions at various adsorption sites of the catalysts pores [37] and confinement effects. Assuming confinement effect can be neglected or are similar across the different catalyst samples investigated, higher T_1/T_2 values usually indicate high surface adsorption interactions between the probe molecules and catalysts [104]. This data can be used to explain the molecular dynamics and adsorption properties of fluids within the studied catalysts HY(5), 1Pt/Cal/HY, and $1Pt^0HY$ [37,104].

The relaxation plot of the bulk molecules is represented in **Fig. S9** with the relaxation ratios close to 1 within 5% experimental error, as expected from the theory, due to the absence of confinement effect or surface interactions [105]. This agrees with reports from literature whereby $T_1 = T_2$ is reported for non-viscous liquids [106]. However, in the case of liquids confined in porous media, these relaxation time constants depend on surface chemistry and morphological/textural properties of the pore network. **Figs. S10** and **S11** highlights the relaxation plots for the HY(5), and 1Pt/Cal/HY catalysts, while that of $1Pt^0HY$ is shown in Fig. 7 as an example of a typical data set.

Functionalization of the zeolites with a bifunctional metal support has a marked effect on surface interactions of different solvents, as shown by the results in Fig. 7c. Experiments were repeated three times and similar results were recorded in all cases confirming the robustness of the results.

In general, the following trend for surface interactions is observed, except for squalene:

$HY\ (5) < 1Pt/Cal/HY < 1Pt^0HY$

This implies that the introduction of platinum and its subsequent

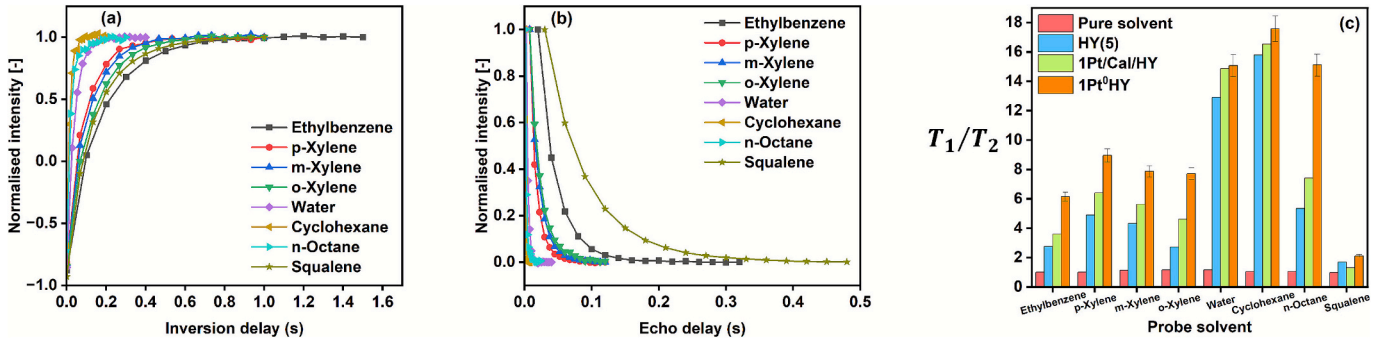

Fig. 7. NMR relaxation plots $1Pt^0HY$ molecules (a) spin-lattice T_1 (b) spin-spin T_2 (c) NMR T_1/T_2 ratios of bulk and probed molecules; curves are fitted to Eqs. S1 and S2 for spin-lattice and spin-spin relaxation respectively.

activation under hydrogen enhances interaction and surface affinity between the surface and the probe molecules. This can be attributed to the increased number of both mesopore volumes occasioned by their metal active sites [107]. The results in Fig. 7c clearly show the strength of interaction in terms of relaxation ratio (T_1/T_2) in the pattern:

Cyclohexane (**17.6**) > **Water** (**15.1**) > ***n*** − **Octane** (**15.1**) > ***p*** − **Xylene** (**9.0**) > ***m*** − **Xylene** (**7.9**) > ***o*** − **Xylene** (**7.7**) > **Ethylbenzene** (**6.2**) > **Squalene** (**2.1**)

→

Decreasing order of surface interactions for $1Pt^0HY$ **catalysts**

The T_1/T_2 values of cyclohexane is the highest (~18), which could be explained by the possibility of the 6-carbon ring cyclohexane molecule with a molecule diameter of ~6 Å [108] been tightly confined and adsorbed within the 6.6 Å size of the sodalite cage of the zeolite framework [109]. The high affinity of water molecules can be explained by considering surface interaction effects, in particular by the ability of water to form strong hydrogen bonding interactions with the framework oxygen present in BAS, as previously reported [37]; in addition, there can be further effects related to the accessibility of water to both large supercages and small β-cages of the faujasite cavities [110]. It is interesting to note the higher T_1/T_2 values of cyclohexane compared to water, despite the cyclohexane being weakly interacting compared to water. This suggests that confinement effects are significant when cyclohexane is confined inside the zeolite cages. A high T_1/T_2 value is observed with *n*-octane, a saturated long chain non-polar hydrocarbon, for the $1Pt^0HY$ (15.1) catalysts, relative to the bare HY zeolite and the 1Pt/Cal/HY. This suggests that the presence of reduced Pt metal particles is enhancing the interactions with the hydrocarbon molecules. The effect of zeolite Al framework in guest-host interactions has been reported by D'Agostino et al. [37] and Brauer et al. [40] using Density Functional Theory (DFT) calculations whereby the surface interactions are studied on atomic level. The relaxation ratio obtained for squalene, an organic compound with the formula $C_{30}H_{50}$ is 2.1, which is a much lower value compared to *n*-octane, another aliphatic hydrocarbon. The low relaxation ratios obtained for squalene can be attributed to its long carbon chain C_{30}, hence the molecule is unable to easily access the zeolite catalyst pores and confinement effects influencing NMR relaxation can be neglected.

The T_1/T_2 values of the xylenes isomers range between 7 and 9, which are lower than the value for cyclohexane. Similarly to squalene, this could be attributed to accessibility issues as xylene isomers do not easily enter the zeolite pores, hence they experience a faster molecular dynamic in the inter-cage space of the zeolite structure. The effect of stearic hindrance, however, comes into play for these isomers whereby the surface interactions with the probe molecules reduces with the location of the two methyl groups on the benzene ring (1,4- > 1,3- > 1,2-) in decreasing order of kinetic diameter [111]. Ethylbenzene, another aromatic A_8 molecule, showed a lower T_1/T_2 ratio (6.2) compared to the xylenes (<7.7). This reduction could be due to weaker surface interaction due to the presence of an ethyl group rather than two methyl groups (in the case of the xylenes). Although, the ethyl group has a higher positive inductive effect (compared to methyl), its attachment to a conjugated aromatic ring produced a less hyperconjugation effect [112] compared to the xylenes, thus leading to a reduction in surface interactions.

D'Agostino et al. [37] reported that the adsorption energy between polar/non-polar guests and their zeolite hosts represents the total energy of interaction which considers: (i) electrostatic interactions between the probe molecules and the BAS of the zeolites; (ii) the dispersion forces on the probe molecules being exerted by the confining environment and unrelated to the acidic strength of the host. Therefore, either of these factors could be the major criterion in explaining the guest-host interactions. It is imperative to understand that the selectivity of a zeolite catalyst is influenced by other factors such as the molecular orientation associated with the spatial arrangement of these molecules, their transition states, interactions of the sorbed molecules with available acid protons or lattice defects [110], in addition to adsorption and confinement effects. These molecular motions could be a singular axis rotation, isotropic or complex reorientations, or translational [109,110]. They are often expressed in the form of quadruple interactions of the molecular nuclei being measured, or at the zeolite walls, or as a result of the dipole-dipole interactions in the sorbed molecules.

4. Conclusion

The hydrocracking of PS with different bifunctional catalysts have been examined and the effects of variation in reaction parameters on conversion and product selectivity have been reported. Changes in product distribution are also explained in the presence and absence of metal nanoparticles on the catalyst supports. The presence of the metal sites introduces more mesoporosity, which enhances the diffusion of the molten polymer, thus promoting hydrogenation reactions of PS. The impregnation of Pt and Ru on the zeolites led to enhanced selectivity

towards the desirable LPG and ethylbenzene, another major industrial liquid feedstock used in the production of many chemicals. Reaction pressure significantly influenced conversion, while reaction time and amount of catalyst altered selectivity and product distribution. The pore structures were found to influence the stability and acidity of the catalysts, as well as the amount of coke adsorbed. The reusability of the bifunctional catalysts was established after identical conversion rate of ethylbenzene with four repeated cycles of $1Pt^0HY$, a desirable indicator towards real-life plastics processing. NMR relaxation T_1/T_2 ratios were used to explain the guest-host interactions and confinement effects and how metal impregnation significantly enhances the activity of a zeolite catalyst.

Our work provides a novel approach towards understanding adsorbate-adsorbent interactions in microporous zeolite structures using NMR relaxation times, with catalytic applications in polystyrene waste recycling. Given the seemingly non-biodegradability of these plastic wastes and its tendency to occupy large volume of landfill space, its chemical recycling targeted towards the selective catalytic conversion into value-added products is a sustainable and economically viable waste management control strategy. In addition, the major gaseous products are good sources of gas for refinery fuels, while the major liquid product, ethylbenzene, is regarded as a good solvent suitable as potential substitute for some industrial feed stocks, and in the production of other chemicals.

CRediT authorship contribution statement

Olajumoke Alabi-Babalola: Writing – review & editing, Writing – original draft, Validation, Resources, Project administration, Methodology, Investigation, Funding acquisition, Formal analysis, Data curation, Conceptualization. **Edidiong Asuquo:** Writing – review & editing, Validation, Project administration, Methodology, Investigation, Formal analysis, Data curation, Conceptualization. **Hassan Alhassawi:** Writing – review & editing, Methodology, Investigation, Formal analysis, Data curation. **Mujtba Alnasser:** Writing – review & editing, Resources, Methodology, Investigation, Formal analysis. **Amal Nadri:** Writing – review & editing, Resources, Methodology, Investigation, Formal analysis. **Sarayute Chansai:** Writing – review & editing, Resources, Methodology, Formal analysis, Data curation. **Carmine D'Agostino:** Writing – review & editing, Validation, Supervision, Resources, Project administration, Methodology, Investigation, Funding acquisition, Formal analysis, Data curation, Conceptualization. **Arthur Garforth:** Writing – review & editing, Validation, Supervision, Resources, Project administration, Methodology, Investigation, Funding acquisition, Formal analysis, Data curation, Conceptualization.

Declaration of competing interest

Dr Olajumoke Alabi-Babalola reports financial support was provided by The Petroleum Technology Development Fund (PTDF), Nigeria. If there are other authors, they declare that they have no known competing financial interests or personal relationships that could have appeared to influence the work reported in this paper.

Acknowledgements

Dr Olajumoke Alabi-Babalola would like to thank the Petroleum Technology Development Fund (PTDF), Nigeria for funding her PhD programme. The authors would like to thank Prof. Chris Hardacre for access to the FTIR-DRIFT facility. This work is also supported by Henry Royce Institute for Advanced Materials funded through EPSRC grants EP/R00661X/1, EP/S019367/1, EP/P025021/1 and EP/P025498/1. The authors would also like to acknowledge Verder Scientific UK Ltd. for access to the BELCAT II/TPD/TPO/TPR instrument.

Appendix A. Supplementary data

Supplementary data to this article can be found online at https://doi.org/10.1016/j.fuproc.2025.108364.

Data availability

Data will be made available on request.

References

[1] X. Zhang, et al., Catalysis as an enabling science for sustainable polymers, Chem. Rev. 118 (2) (2018) 839–885.
[2] A.A. Bin Jumah, A. Tedstone, A.A. Garforth, Hydrocracking of virgin and post-consumer polymers, Microporous Mesoporous Mater. 315 (2021) 110912.
[3] APME, Plastics-The Facts 2019, Association of Plastic Manufacturers in Europe, 2019.
[4] OECD, Global Plastics Outlook, in Economic Drivers, Environmental Impacts and Policy Options: Paris, 2022.
[5] J. Hopewell, R. Dvorak, E. Kosior, Plastics recycling: challenges and opportunities, Philos. Trans. R. Soc. B 364 (1526) (2009) 2115–2126.
[6] I. Vollmer, et al., Beyond mechanical recycling: giving new life to plastic waste, Angew. Chem. Int. Ed. 59 (36) (2020) 15402–15423.
[7] O. Alabi-Babalola, E. Aransiola, T. Shittu, Adsorption and kinetic study of activated carbon produced from post-consumer low-density polyethylene (LDPE) wastes, Adv. Chem. Eng. Sci. 11 (01) (2021) 38.
[8] O. Alabi-Babalola, E. Aransiola, T. Shittu, A study on the optimization and adsorption capacity of activated carbon produced from polyvinyl chloride (PVC) wastes, Ife J. Technol. 26 (1) (2019) 34–46.
[9] M.P. González-Marcos, et al., Optimization of supports in bifunctional supported Pt catalysts for polystyrene hydrocracking to liquid fuels, Top. Catal. 64 (2021) 224–242.
[10] Z. Dong, et al., Understanding the structure–activity relationships in catalytic conversion of polyolefin plastics by zeolite-based catalysts: a critical review, ACS Catal. 12 (24) (2022) 14882–14901.
[11] M.-Q. Zhang, et al., Catalytic strategies for upvaluing plastic wastes, Chem 8 (11) (2022) 2912–2923.
[12] L. Gan, et al., Beyond conventional degradation: catalytic solutions for polyolefin upcycling, CCS Chem. 6 (2) (2024) 313–333.
[13] A. Adrados, et al., Pyrolysis of plastic packaging waste: a comparison of plastic residuals from material recovery facilities with simulated plastic waste, Waste Manag. 32 (5) (2012) 826–832.
[14] S. Al-Salem, et al., A review on thermal and catalytic pyrolysis of plastic solid waste (PSW), J. Environ. Manag. 197 (2017) 177–198.
[15] A.F. Anene, et al., Experimental study of thermal and catalytic pyrolysis of plastic waste components, Sustainability 10 (11) (2018) 3979.
[16] S. Budsaereechai, A.J. Hunt, Y. Ngernyen, Catalytic pyrolysis of plastic waste for the production of liquid fuels for engines, RSC Adv. 9 (10) (2019) 5844–5857.
[17] H. Gulab, et al., Plastic catalytic pyrolysis to fuels as tertiary polymer recycling method: effect of process conditions, J. Environ. Sci. Health A 45 (7) (2010) 908–915.
[18] P.A. Kots, et al., Electronic modulation of metal-support interactions improves polypropylene hydrogenolysis over ruthenium catalysts, Nat. Commun. 13 (1) (2022) 5186.
[19] C. Wang, et al., Polyethylene hydrogenolysis at mild conditions over ruthenium on tungstated zirconia, JACS Au 1 (9) (2021) 1422–1434.
[20] C. Wang, et al., A general strategy and a consolidated mechanism for low-methane hydrogenolysis of polyethylene over ruthenium, Appl. Catal. B Environ. 319 (2022) 121899.
[21] A. Bin Jumah, et al., Catalyzing the hydrocracking of low density polyethylene, Ind. Eng. Chem. Res. 58 (45) (2019) 20601–20609.
[22] Z. Chen, B.J. Erwin, L. Che, Hydrocracking of polyethylene to hydrocarbon fuels over Pt/USY catalysts: assessment of the hydrogen donors, J. Clean. Prod. 424 (2023) 138861.
[23] J. Huang, et al., Chemical recycling of plastic waste for sustainable material management: a prospective review on catalysts and processes, Renew. Sust. Energ. Rev. 154 (2022) 111866.
[24] L.O. Mark, M.C. Cendejas, I. Hermans, The use of heterogeneous catalysis in the chemical valorization of plastic waste, ChemSusChem 13 (22) (2020) 5808–5836.
[25] X. Wei, et al., Tandem oxidative and thermal cracking of polypropylene at low temperatures, Mater. Horiz. 10 (9) (2023) 3694–3701.
[26] Z. Zhang, et al., Chemical recycling of waste polystyrene into styrene over solid acids and bases, Ind. Eng. Chem. Res. 34 (12) (1995) 4514–4519.
[27] H. Ukei, et al., Catalytic degradation of polystyrene into styrene and a design of recyclable polystyrene with dispersed catalysts, Catal. Today 62 (1) (2000) 67–75.
[28] J.-S. Kim, et al., Degradation of polystyrene waste over base promoted Fe catalysts, Catal. Today 87 (1–4) (2003) 59–68.
[29] O.S. Woo, N. Ayala, L.J. Broadbelt, Mechanistic interpretation of base-catalyzed depolymerization of polystyrene, Catal. Today 55 (1–2) (2000) 161–171.
[30] H. Ke, et al., Reaction mechanism of styrene monomer recovery from waste polystyrene by supercritical solvents, Polym. Degrad. Stab. 89 (2) (2005) 312–316.

[31] W. Bajdur, et al., Effective polyelectrolytes synthesised from expanded polystyrene wastes, Eur. Polym. J. 38 (2) (2002) 299–304.
[32] Y. Liu, J. Qian, J. Wang, Pyrolysis of polystyrene waste in a fluidized-bed reactor to obtain styrene monomer and gasoline fraction, Fuel Process. Technol. 63 (1) (2000) 45–55.
[33] I.M. Maafa, Pyrolysis of polystyrene waste: a review, Polymers 13 (2) (2021) 225.
[34] S. Fan, et al., Microwave-assisted pyrolysis of polystyrene for aviation oil production, J. Anal. Appl. Pyrolysis 162 (2022) 105425.
[35] N.D. Hesse, R.L. White, Polyethylene catalytic hydrocracking by PtHZSM-5, PtHY, and PtHMCM-41, J. Appl. Polym. Sci. 92 (2) (2004) 1293–1301.
[36] R. Ochoa, et al., Catalytic degradation of medium density polyethylene over silica-alumina supports, Fuel Process. Technol. 49 (1–3) (1996) 119–136.
[37] C. D'Agostino, et al., Adsorbate/adsorbent interactions in microporous zeolites: mechanistic insights from NMR relaxation and DFT calculations, Mater. Today Chem. 29 (2023) 101443.
[38] J. Korb, Nuclear magnetic relaxation of liquids in porous media, New J. Phys. 13 (3) (2011) 035016.
[39] C. D'Agostino, et al., Assessing the effect of reducing agents on the selective catalytic reduction of NO x over Ag/Al 2 O 3 catalysts, Cat. Sci. Technol. 6 (6) (2016) 1661–1666.
[40] P. Bräuer, et al., Effect of Al content on the strength of terminal silanol species in ZSM-5 zeolite catalysts: a quantitative DRIFTS study without the use of molar extinction coefficients, Phys. Chem. Chem. Phys. 20 (6) (2018) 4250–4262.
[41] J.A. Lercher, C. Gründling, G. Eder-Mirth, Infrared studies of the surface acidity of oxides and zeolites using adsorbed probe molecules, Catal. Today 27 (3–4) (1996) 353–376.
[42] C. Le Minh, et al., Temperature-programmed oxidation of coke deposited on cracking catalysts: combustion mechanism dependence, Energy Fuel 11 (2) (1997) 463–469.
[43] A. Camiloti, et al., Acidity of Beta zeolite determined by TPD of ammonia and ethylbenzene disproportionation, Appl. Catal. A Gen. 182 (1) (1999) 107–113.
[44] M. Niwa, N. Katada, New method for the temperature-programmed desorption (TPD) of ammonia experiment for characterization of zeolite acidity: a review, Chem. Rec. 13 (5) (2013) 432–455.
[45] O.A. Abdelrahman, et al., Simple quantification of zeolite acid site density by reactive gas chromatography, Cat. Sci. Technol. 7 (17) (2017) 3831–3841.
[46] W. Yang, et al., Advances in development and industrial applications of ethylbenzene processes, Chin. J. Catal. 37 (1) (2016) 16–26.
[47] U.K. Indexbox, Ethylbenzene-Market Analysis, Forecast, Size, Trends and Insights, 2023.
[48] J. Paulik, F. Paulik, E. Czaran, The thermal decomposition of platinum tetrammine chloride, Anal. Chim. Acta 101 (2) (1978) 409–412.
[49] C. Fuentes, et al., Analysis of the emission of PAH in the thermal and catalytic pyrolysis of polystyrene, Catal. Today 372 (2021) 175–182.
[50] G. Ali, et al., Thermo-catalytic decomposition of polystyrene waste: comparative analysis using different kinetic models, Waste Manag. Res. 38 (2) (2020) 202–212.
[51] A.M. Gonzalez-Aguilar, et al., Effects of heating rate and temperature on the thermal pyrolysis of expanded polystyrene post-industrial waste, Polymers 14 (22) (2022) 4957.
[52] I. Kremer, et al., Catalytic decomposition and kinetic study of mixed plastic waste, Clean Techn. Environ. Policy 23 (2021) 811–827.
[53] I. Kremer, et al., Catalytic pyrolysis of mechanically non-recyclable waste plastics mixture: kinetics and pyrolysis in laboratory-scale reactor, J. Environ. Manag. 296 (2021) 113145.
[54] H.R. Azimi, M. Rezaei, F. Majidi, The non-isothermal degradation kinetics of St–MMA copolymers, Polym. Degrad. Stab. 99 (2014) 240–248.
[55] F.C. Lírio, et al., Kinetics of poly (vinyl chloride) thermal degradation by ionizing radiation, Cadernos UniFOA 15 (44) (2020).
[56] A. Benarbia, et al., Synthesis, characterization and thermal degradation kinetics of copolyesters, J. Mater. Environ. Sci. 5 (4) (2014) 1262–1279.
[57] O. Omosola, et al., On the thermogravimetric analysis of polymers: polyethylene oxide powder and nanofibers, J. Appl. Polym. Sci. 139 (18) (2022) 52055.
[58] Y. Ha, J. Jeon, Thermogravimetric analysis and pyrolysis characterization of expanded–polystyrene and polyurethane–foam insulation materials, Case Stud. Therm. Eng. 54 (2024) 104002.
[59] K. Akçay, et al., Wet ball milling of zeolite HY, Powder Technol. 142 (2–3) (2004) 121–128.
[60] B. Zhuman, S.F. Anis, R. Hashaikeh, Obtaining high crystalline ball milled HY zeolite particles with carbon nanostructures as a damping material, Microporous Mesoporous Mater. 273 (2019) 19–25.
[61] Y. Zhang, et al., Structure and catalytic properties of the Zn-modified ZSM-5 supported platinum catalyst for propane dehydrogenation, Chem. Eng. J. 270 (2015) 352–361.
[62] E. Gharibshahi, E. Saion, Influence of dose on particle size and optical properties of colloidal platinum nanoparticles, Int. J. Mol. Sci. 13 (11) (2012) 14723–14741.
[63] R. Insyani, et al., RuO2–Ru/Hβ zeolite catalyst for high-yield direct conversion of xylose to tetrahydrofurfuryl alcohol, Appl. Catal. B Environ. 291 (2021) 120120.
[64] C.V. Hidalgo, et al., Measurement of the acidity of various zeolites by temperature-programmed desorption of ammonia, J. Catal. 85 (2) (1984) 362–369.
[65] N. Robinson, C. D'agostino, M.L. Johns, Functional group resolved NMR relaxation of 3-carbon adsorbates in mesoporous alumina, Magnetic Resonance Letters 3 (3) (2023) 248–255.
[66] E. Paparazzo, On the interpretation of XPS spectra of metal (Pt, Pt–Sn) nanoparticle/graphene systems, Carbon 63 (2013) 578–581.
[67] C.D. Wagner, NIST X-Ray Photoelectron Spectroscopy Database. NIST Standarad Reference Database 20, 2000.
[68] C. Wagner, et al., NIST X-Ray Photoelectron Spectroscopy Database, NIST Standard Reference Database 20, Version 3.4 (Web Version), US Department of Commerce, 2003, p. 1.
[69] J. Rumble Jr., D. Bickham, C. Powell, The NIST x-ray photoelectron spectroscopy database, Surf. Interface Anal. 19 (1−12) (1992) 241–246.
[70] D. Chichova, et al., X-ray photoelectron spectroscopy investigation of Pd-beta zeolite catalysts with different acidities, Top. Catal. 52 (2009) 359–379.
[71] B. Schleich, D. Schmeisser, W. Göpel, Structure and reactivity of the system Si/SiO2/Pd: a combined XPS. UPS and HREELS study, Surf. Sci. 191 (3) (1987) 367–384.
[72] Z. Bastl, L. Kubelková, J. Nováková, XPS study of Pt ammine decomposition in K faujasites: comparison with bulk behavior, Zeolites 19 (4) (1997) 279–287.
[73] G. Zhang, D. Yang, E. Sacher, X-ray photoelectron spectroscopic analysis of Pt nanoparticles on highly oriented pyrolytic graphite, using symmetric component line shapes, J. Phys. Chem. C 111 (2) (2007) 565–570.
[74] X. Fu, et al., Surface modification of small platinum nanoclusters with alkylamine and alkylthiol: an XPS study on the influence of organic ligands on the Pt 4f binding energies of small platinum nanoclusters, J. Colloid Interface Sci. 243 (2) (2001) 326–330.
[75] C. Chen, et al., Enhanced performance in catalytic combustion of toluene over mesoporous beta zeolite-supported platinum catalyst, Appl. Catal. B Environ. 140 (2013) 199–205.
[76] J. Xu, et al., Mechanistic study of preferential CO oxidation on a Pt/NaY zeolite catalyst, J. Catal. 287 (2012) 114–123.
[77] P.S. Bagus, E.S. Ilton, C.J. Nelin, The interpretation of XPS spectra: insights into materials properties, Surf. Sci. Rep. 68 (2) (2013) 273–304.
[78] B.V. Crist, XPS in industry—problems with binding energies in journals and binding energy databases, J. Electron Spectrosc. Relat. Phenom. 231 (2019) 75–87.
[79] S. Bailleul, et al., A supramolecular view on the cooperative role of Brønsted and Lewis acid sites in zeolites for methanol conversion, J. Am. Chem. Soc. 141 (37) (2019) 14823–14842.
[80] G. Woolery, et al., On the nature of framework Brønsted and Lewis acid sites in ZSM-5, Zeolites 19 (4) (1997) 288–296.
[81] S. Li, et al., Brønsted/Lewis acid synergy in dealuminated HY zeolite: a combined solid-state NMR and theoretical calculation study, J. Am. Chem. Soc. 129 (36) (2007) 11161–11171.
[82] N. Viswanadham, et al., Catalytic properties of nano-sized ZSM-5 aggregates, Catal. Today 141 (1–2) (2009) 182–186.
[83] M. Remy, G. Poncelet, A new approach to the determination of the external surface and micropore volume of zeolites from the nitrogen adsorption isotherm at 77 K, J. Phys. Chem. 99 (2) (1995) 773–779.
[84] P. Voogd, J. Scholten, H. Van Bekkum, Use of the t-plot—De Boer method in pore volume determinations of ZSM-5 type zeolites, Colloids Surf. A Physicochem. Eng. Asp. 55 (1991) 163–171.
[85] A. Zachariou, et al., Counting the acid sites in a commercial ZSM-5 zeolite catalyst, ACS Phys. Chem. Au 3 (1) (2022) 74–83.
[86] K. Sato, et al., Role of HY zeolite mesopores in hydrocracking of heavy oils, J. Catal. 200 (2) (2001) 288–297.
[87] W. Ding, J. Liang, L.L. Anderson, Hydrocracking and hydroisomerization of high-density polyethylene and waste plastic over zeolite and silica− alumina-supported Ni and Ni− Mo sulfides, Energy Fuel 11 (6) (1997) 1219–1224.
[88] Z. Qiu, et al., A reusable, impurity-tolerant and noble metal–free catalyst for hydrocracking of waste polyolefins, Sci. Adv. 9 (25) (2023) eadg5332.
[89] K. Möller, T. Bein, Mesoporosity–a new dimension for zeolites, Chem. Soc. Rev. 42 (9) (2013) 3689–3707.
[90] D. Olson, et al., Crystal structure and structure-related properties of ZSM-5, J. Phys. Chem. 85 (15) (1981) 2238–2243.
[91] D. Trueba, et al., Product composition and coke deposition in the hydrocracking of polystyrene blended with vacuum gasoil, Fuel Process. Technol. 224 (2021) 107010.
[92] E.G. Fuentes-Ordóñez, et al., Mechanism and kinetics in catalytic hydrocracking of polystyrene in solution, Polym. Degrad. Stab. 124 (2016) 51–59.
[93] E.G. Fuentes-Ordonez, et al., Transport phenomena in catalytic hydrocracking of polystyrene in solution, Ind. Eng. Chem. Res. 52 (42) (2013) 14798–14807.
[94] D. Trueba, et al., Kinetic modeling of the hydrocracking of polystyrene blended with vacuum gasoil, Chem. Eng. J. 451 (2023) 138709.
[95] Z. Zhang, et al., Cascade upcycling polystyrene waste into ethylbenzene over Fe2N@ C, Appl. Catal. B Environ. 323 (2023) 122164.
[96] E. Fuentes, et al., Polystirene hydrocracking in solution over bifunctional catalysts, in: Proceedings of the 6th International Symposium on Feedstock Recycling of Polymeric Materials. Toledo, Spain, 2011.
[97] L. Wang, J. Xiao, Hydrogen-Atom Transfer Reactions: Hydrogen Transfer Reactions: Reductions and Beyond, 2016, pp. 205–259.
[98] J. Sun, et al., Solubility measurement of hydrogen, ethylene, and 1-hexene in polyethylene films through an intelligent gravimetric analyzer, J. Appl. Polym. Sci. 134 (8) (2017).
[99] A. Guyot, Recent developments in the thermal degradation of polystyrene—a review, Polym. Degrad. Stab. 15 (3) (1986) 219–235.
[100] J. Fals, et al., A comprehensive study of product distributions and coke deposition during catalytic cracking of vacuum gas oil over hierarchical zeolites, Heliyon 9 (4) (2023).

[101] B.C. Vance, et al., Single pot catalyst strategy to branched products via adhesive isomerization and hydrocracking of polyethylene over platinum tungstated zirconia, Appl. Catal. B Environ. 299 (2021) 120483.
[102] R. Lin, R.L. White, Acid-catalyzed cracking of polystyrene, J. Appl. Polym. Sci. 63 (10) (1997) 1287–1298.
[103] F. Ortega García, E. Mar Juárez, Heavy oil hydrocracking on a liquid catalyst, Energy Fuel 31 (8) (2017) 7995–8000.
[104] C. D'Agostino, et al., Interpretation of NMR relaxation as a tool for characterising the adsorption strength of liquids inside porous materials, Chem Eur J 20 (40) (2014) 13009–13015.
[105] R.J. Abraham, Nuclear Magnetic Resonance Vol. 7, Royal Society of Chemistry, 1973.
[106] N. Robinson, et al., Nuclear spin relaxation as a probe of zeolite acidity: a combined NMR and TPD investigation of pyridine in HZSM-5, Phys. Chem. Chem. Phys. 23 (33) (2021) 17752–17760.
[107] X. Zhu, et al., Catalytic cracking of C4 alkenes to propene and ethene: influences of zeolites pore structures and Si/Al2 ratios, Appl. Catal. A Gen. 288 (1–2) (2005) 134–142.
[108] G. Dosseh, Y. Xia, C. Alba-Simionesco, Cyclohexane and benzene confined in MCM-41 and SBA-15: confinement effects on freezing and melting, J. Phys. Chem. B 107 (26) (2003) 6445–6453.
[109] J.A. Incavo, P.K. Dutta, Zeolite host-guest interactions: optical spectroscopic properties of tris (bipyridine) ruthenium (II) in zeolite Y cages, J. Phys. Chem. 94 (7) (1990) 3075–3081.
[110] H. Lechert, W. Basler, Molecular motion in zeolite sorbends, studied by various NMR methods, J. Phys. Chem. Solids 50 (5) (1989) 497–521.
[111] Y. Yang, P. Bai, X. Guo, Separation of xylene isomers: a review of recent advances in materials, Ind. Eng. Chem. Res. 56 (50) (2017) 14725–14753.
[112] R.A. Benkeser, R.A. Hickner, D.I. Hoke, The inductive effects of alkyl groups as determined by desilylation reactions, J. Am. Chem. Soc. 80 (9) (1958) 2279–2282.